Emergence of cooperative rotor dynamics in metal–organic frameworks via tuned steric interactions

Adrian Gonzalez-Nelson,[1,2] Srinidhi Mula,[1] Mantas Šimėnas,[3] Sergejus Balčiūnas,[3] Adam R. Altenhof,[4,5] Cameron S. Vojvodin,[4,5] Jūras Banys,[3] Robert W. Schurko,[4,5]* François-Xavier Coudert,[6]* and Monique A. van der Veen[1]*

[1]Department of Chemical Engineering, Delft University of Technology, The Netherlands. [2]DPI, P.O.Box 92, 5600 AX Eindhoven, The Netherlands. [3]Faculty of Physics, Vilnius University, Vilnius, Lithuania. [4]Department of Chemistry and Biochemistry, Florida State University, Tallahassee, FL, USA. [5]National High Magnetic Field Laboratory, Tallahassee, FL, USA. [6]Chimie ParisTech, PSL University, CNRS, Institut de Recherche de Chimie Paris, Paris, France.

*Correspondence: fx.coudert@chimieparistech.psl.eu; M.A.vanderVeen@tudelft.nl; rschurko@fsu.edu

Abstract

The organic components in metal-organic frameworks (MOFs) enjoy a unique situation: they are embedded in a crystalline lattice, yet, as they are separated from each other by tunable free space, a large variety of dynamic behavior can emerge. These rotational dynamics of the organic linkers are especially important due to their influence over properties such as gas adsorption and kinetics of guest release. In order to fully exploit linker rotation, it is necessary to engineer correlated linker dynamics to achieve their cooperative functional motion. Here, we show that for MIL-53, a topology with closely spaced rotors, the phenylene functionalization allows to tune the rotors' steric environment, shifting linker rotation from completely static to rapid motions at frequencies above 100 MHz. For steric interactions that start to inhibit independent rotor motion, we identify for the first time the emergence of correlated rotation modes in linker dynamics. These findings pave the way for function-specific engineering of gearlike cooperative motion in MOFs.

Main

The hybrid nature of metal–organic frameworks (MOFs) goes hand in hand with diverse and often complex behavior. The dynamic traits of these materials are increasingly capturing the curiosity of researchers in the field: MOFs show the potential of displaying intricate dynamics, similar to that observed in other materials built from closely interacting molecules, such as crowded movement of proteins in lipid bilayers[1,2] or concerted molecular motion in liquid crystals.[3] The organic components in MOFs are embedded in a crystalline lattice, yet, in contrast to traditional molecular crystals, they are separated from each other by modifiable free space, providing a handle to tune dynamic behavior in an ordered and stable supramolecular arrangement.[4–6]

A decade ago, Yaghi and Stoddart proposed that 'robust dynamics' could be achieved by mechanically interlocking organic components onto the linkers, such that they have the necessary freedom of mobility without compromising the MOF structure.[7] Since then, it has become evident that stable frameworks that display inherent rotational motion are in fact ubiquitous.[8,9] However, not all such frameworks are usable in practice, and the performance of a MOF in specific applications is highly dependent on its dynamic properties, a prime example being adsorption behavior in flexible MOFs.[10–15] Furthermore, MOF-based crystalline molecular machines will require external control of linker motion, making the engineering of correlated dynamics a necessary step to achieve cooperative functional mobility.[5,6,16,17]

Recent achievements in rotor-MOFs include engineering ultrafast rotation by decreasing the rotation energy barrier via molecular design,[18,19] reaching rates as high as those in gas or liquid phases. Additionally, the first example of unidirectional rotation in MOF linkers by the Feringa group[20] represents a crucial step towards attaining nanomotors embedded in a crystalline lattice that can produce useful work.[21] A recent study on rotor-MOFs presented evidence of steric interactions between rotating phenylene units within a single linker.[22] Yet, the understanding, let alone the engineering, of correlated dynamics based on steric interactions between linkers remains extremely limited.

The growing field of rotor-MOFs may benefit from inspiration drawn from the more developed field of crystalline molecular rotors. In many such systems, it has been found that in structures where rotor–rotor distances are small enough, the resulting steric interactions force the rotational dynamics to adopt correlated gearlike mechanisms.[23–26] Here, we present for the first time how correlated motions emerge in linker dynamics as the steric environment of the rotors is gradually modified. We use linker functionalization in the MIL-53 family of materials to tune both the pore dimensions and the rotor–rotor interactions. The MIL-53 topology proves to be an excellent choice due to its functionalization-dependent pore size configurations, i.e., the metastability of two phases, large pore and narrow pore. Moreover, terephthalate-based organic linkers are very common among MOFs.

Results and discussion

To start, we focus on the intramolecular effects of linker functionalization on rotational motion. In terephthalate linkers, the benzene rings can rotate with respect to the carboxyl groups, which are fixed due to their coordination to the metal nodes. The maximum energy corresponds to a conformation where the benzene rings form a 90° angle with both carboxyl groups,[27–29] as the overlap between the *p* orbitals in the ring and in the carboxyl groups is minimized.

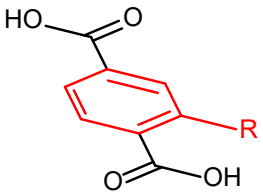

Minimum (ground state)

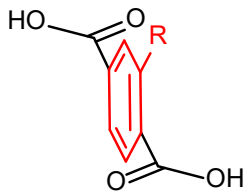

Maximum (transition state)

Table 1. Calculated barriers for 180° rotation on terephthalic acid and its derivatives.

R	ΔE_{rot} / kJ mol^{-1} †
H	47.7
hydroxy	64.2
amino	53.7
methoxy	42.1
cyano	34.5
fluoro	35.9
chloro	25.0
bromo	25.1
nitro	17.1

†The maximum energy state for each molecule (E_{90}) is obtained from constrained geometry optimizations, setting the dihedral angles between carboxylic groups and ring to 90°. Relative values were obtained with respect to a planar conformation energy, see Supplementary Information section 3.1 for details.

We modeled with density functional theory (DFT) calculations the intrinsic rotational energy barriers (ΔE_{rot}) of different functionalized terephthalic acids with different functional groups as the relative energy between the transition state and a planar conformer (Table 1 and Graphic). With respect to the unsubstituted terephthalic acid, most substituent groups decrease the ΔE_{rot} barrier. In these cases,

steric repulsion between the substituent group and the closest carboxyl oxygen likely destabilizes the planar configuration,[25,30] decreasing the energy difference between the transition state and the ground state. This effect is particularly significant in the nitro-substituted molecule (Supplementary Fig. 1), where the rotation barrier is the lowest at ΔE_{rot} = 17.1 kJ mol^{-1}, i.e., less than 7 kT at room temperature.

Only electron donating substituents, namely amino and hydroxy groups, cause an increase in ΔE_{rot}. We argue that this is in fact mostly due to stabilization via a hydrogen bond with the adjacent carboxylic acid oxygen (1.93 Å for NH···O and 1.75 Å OH···O, see Supplementary Fig. 9). Indeed, simply breaking the H-bond by rotating the hydroxy group by 180° results in an energy penalty of 31 kJ mol^{-1}. Conversely, the electron-donating methoxy substituent without H-bond formation shows a slight decrease in ΔE_{rot}.

Experimental work on MIL-53[31–33] has established that its *p*-phenylene groups undergo rotation in the form of π-flips, exhibiting similar behavior to several other terephthalate-based MOFs.[29,34–36] The large-pore conformation of MIL-53 suggests that the rotating rings should not be subject to significant steric effects. The rotator's closest interactions are between contiguous linkers in the same row (or pore wall): their closest ring-to-ring (-CH···HC-) distance possible is 2.3 Å, which means their van der Waals radii barely overlap. This spacing is limited yet sufficient for unfunctionalized terephthalate rotors to perform full rotations in the form of π-flips, as evidenced experimentally.[32]

This spacing between the linkers in MIL-53 family is still relatively small, in contrast to other MOFs such as IRMOF and UiO-66. This suggests that ring substituents are likely to influence the dynamics of rotors. Based on the DFT calculations of the free linkers, we selected two contrasting groups—nitro and amino—to assess the impact of linker functionalization in the complete framework, a "crowded" environment. Moreover, for MIL-53 materials, functionalization has an important impact on the flexible crystalline conformation: guest-free NO_2-MIL-53(Al) and MIL-53(Al) are present in the large-pore form at ambient conditions, [37,38] while guest-free NH_2-MIL-53(Al) is present in the denser narrow-pore form (Figure 1).[37,39,40] Table 2 presents the characteristic distances between rotors in each form of the framework, showing how the difference in pore opening impacts row-to-row distance, but not rotor spacing within a row. The row-to-row distance of the narrow-pore amino-MOF indicates likely inter-row steric effects prohibiting full rotation of rings. For both functionalized frameworks, steric repulsion between neighboring linkers within the same row is expected.

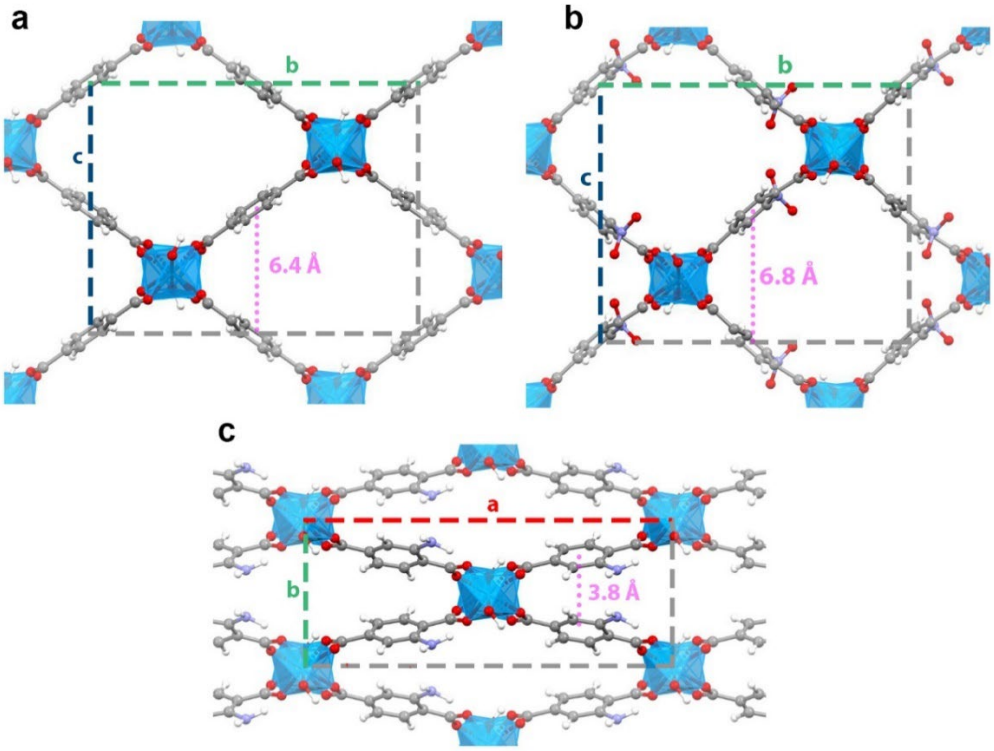

Figure 1. Structure of three members of the MIL-53 family viewed along the pore direction. a, MIL-53(Al), **b**, NO_2-MIL-53(Al), and **c**, NH_2-MIL-53(Al). This topology is characterized by four distinct rows of linkers per unit cell forming rhombic pores. Closest row distances for each MOF are marked in magenta. For compete unit cell parameters see Supplementary Table 1.

Table 2. Unit cell geometry influence on rotor spacing.

MOF	Rotor spacing within row / Å*	Pore rhombus angle / °	Row-to-row distance / Å†
MIL	6.6	75.0	6.4
nitro	6.7	79.5	6.8
amino	6.6	43.8	3.8

* Defined as distance between neighboring C–C rotation axes, see Supplementary Information section 3.2.
† For definition see Supplementary Information section 3.2.

Each crystallographic unit cell contains four linkers. To explore the energy associated with linker rotation, we forced the rotation steps on one linker starting from the global minimum conformation, followed by partial geometry optimization at each step. The rotational space of a nitroterephthalate linker is defined in Figure 2b (for aminoterephthalate see Supplementary Fig. 10). The obtained potential energy curves (or energy profiles as a function of rotation) are shown in Figure 2c. The energy profile of NH_2-MIL-53 shows a very steep increase upon linker rotation, far larger in magnitude than the barrier calculated for the free linker (54 kJ mol^{-1}). This is the result of row-to-row steric hindrance in the tightly packed narrow-pore phase (see Supplementary Fig. 11), indicating that large amplitude rotations are unlikely to occur in this MOF. For NO_2-MIL-53(Al), we find energy minima at ±30° and ±150°, with expected maxima at ±90°, and local maxima at 0° and 180° due to steric effects experienced by the linker in the planar conformation (intramolecular, *vide supra*, and overlap between nitro and a hydrogen atom of the closest adjacent ring). The potential energy maxima of ~ 40 kJ mol^{-1} is in the range of aromatic ring π-flips found in other MOFs,[31,34,35,41,42] which indicates the feasibility of linker rotation.

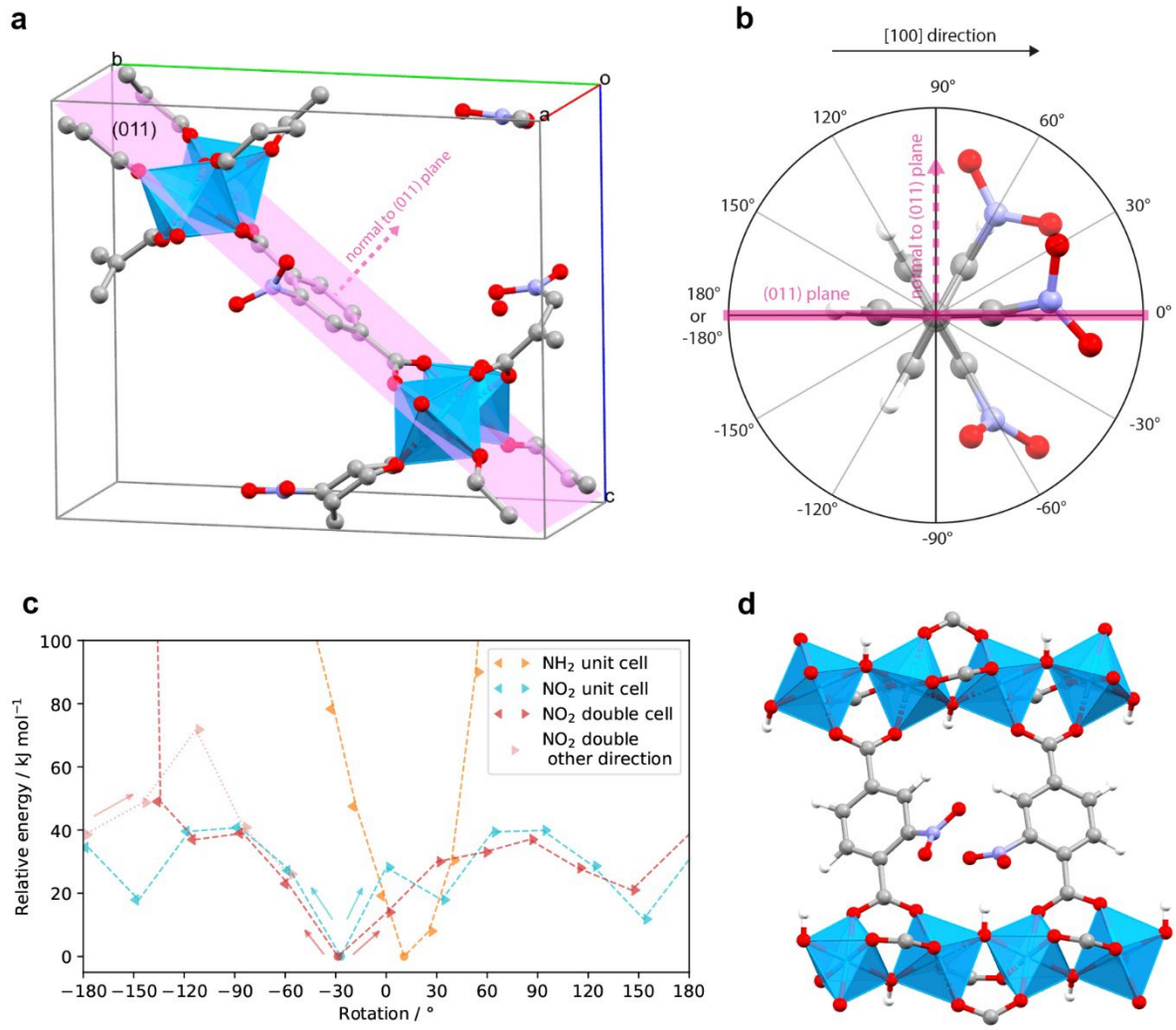

Figure 2. Effect of linker rotation on the potential energy as studied by DFT. a, Unit cell of NO_2-MIL-53(Al) with central linker in 0° rotation with respect to (011) plane (pink); hydrogens omitted for clarity. **b**, Rotation angle is defined as the angle between benzene ring plane and (011) plane, taking 0° as the conformation with the functional group pointing in the positive [100] direction. The sign of the angle is assigned based on the direction normal of the reference plane. **c**, Potential energy profiles for NH_2-MIL-53(Al) and NO_2-MIL-53(Al) single and 2x1x1 supercell. The direction of rotation is indicated by the direction of the marker. **d**, Unfavorable head-to-head nitro group encounter in adjacent linkers in a supercell at –145° rotation.

Nevertheless, these periodic single unit cell calculations force the nitro linkers in a row along [100] to rotate together, as they are periodic images of each other. Such an ordered motion limits other possible interactions between neighboring linkers in the same row. To consider non-synchronous rotation, we calculated the energy profile for the rotation of one linker in a 2x1x1 supercell (Fig. 2c), where the same-row neighbor linker is not constrained and can move independently. Out of several combinations of nitro positions on the pair of rings, we address the one where nitro groups are located on identical carbon positions for each of the two cells. This represents the scenario with most impactful steric effects between two rotors.

Here again, we analyzed both possible directions of rotation, and in most of the rotation space, similar values are found as compared to the single cell calculations. However, negative rotation beyond −120°, where the two nitro groups of same-row neighbors come into close proximity, shows a very steep energy increase due to head-to-head NO_2 interactions that inhibit the rotational mobility (Fig. 2d and Supplementary Fig. 12). Alternatively, when this part of the rotational space is reached via positive

rotation beyond +180°, the same-row neighbor linker is pushed out of the way in a cooperative fashion (Supplementary Fig. 13), meaning that the simultaneous rotation of the neighbor linker makes the rotational event energetically feasible. Rotation in this direction could be described as gearlike: both linkers' nitro groups are in contact and they are both required to rotate simultaneously in order to allow movement.

In the alternative case where nitro groups are not in equivalent carbon positions in the two cells, we obtain profiles with significantly lower energies at angles where the nitro groups approach head-to-head (see Supplementary Figs. 14 and 15). These results indicate that, in contrast to the case of identical pairs, independent rotation of alternatively positioned nitrophenylene neighbors should not be ruled out. Hence, in a real system with disordered nitro positions, varying degrees of rotational mobility may be expected. Due to the size and positioning of its linkers, NO_2-MIL-53 is a framework in which full rotations are energetically feasible, yet are unlikely to occur independently and in certain cases will require cooperativity between the motion of same-row linkers.[23,24,26]

Broadband dielectric spectroscopy (BDS) has proven particularly useful for probing the motion of MOF linkers containing polar functional groups.[43–45] The imaginary part (ε'') of the complex dielectric permittivity ($\varepsilon^* = \varepsilon' - i\varepsilon''$) contains information about the dynamic relaxation processes of dipolar moieties in the dielectric material.[46,47] The temperature and frequency dependences of ε'' for MIL-53(Al), NH_2-MIL-53(Al) and NO_2-MIL-53(Al) are presented in Figure 3 and Supplementary Figure 17. Peaks in ε'' correspond to dielectric losses due to dipolar motion, with the frequency of the maximum of ε'' corresponding to the mean relaxation time of the dipolar motion at that temperature.

NO_2-MIL-53(Al) shows a strong relaxation process with peaks dispersed in terms of both frequency and temperature (Fig. 3a and b), a feature typical of dipolar linker relaxations in MOFs.[44,45,48] In contrast, NH_2-MIL-53(Al) shows no relaxation process (Figure 3c), confirming a strongly hindered environment of the rotors, in correspondence with our DFT results. MIL-53(Al) (Figure 3d) exhibits a very weak dielectric relaxation, even though the mobile *p*-phenylene units do not have a permanent dipole. This may be due to small deformations of the linkers that lead to spontaneous dipole moments, or the presence of polar impurities.[47]

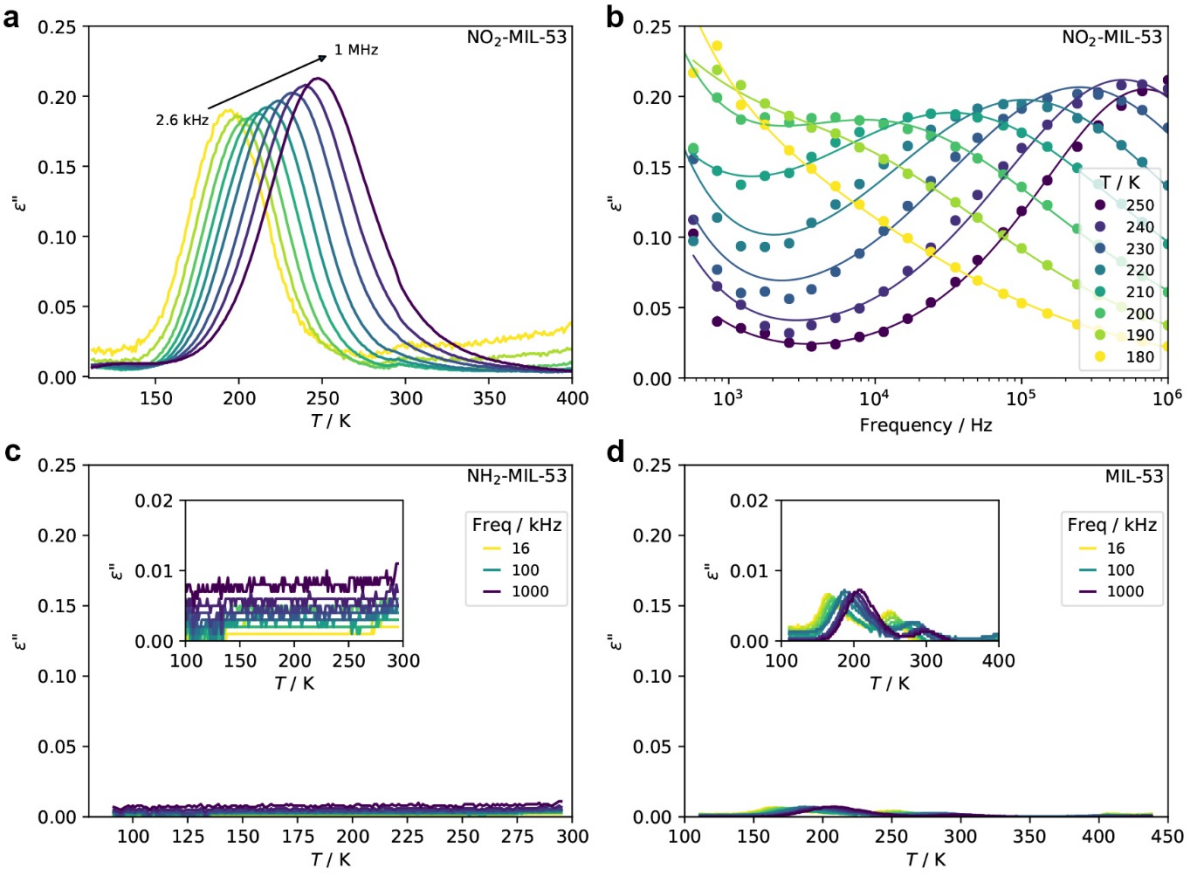

Figure 3. Dielectric spectra of the three systems. a,b, Imaginary part (ε'') of ε^* for NO_2-MIL-53(Al) with respect temperature to (**a**) and frequency (**b**). The latter includes the fitted Cole-Cole model as continuous lines. **c,d,** Temperature dependence of ε'' for NH_2-MIL-53(Al) (c) and MIL-53(Al) (d).

As expected, the dispersion frequency of the nitro linker relaxation increases with temperature, more specifically, from 2.6 kHz at 180 K to 1 MHz at 250 K. The frequency dependence of ε^* at different temperatures was fitted using the Cole-Cole equation (Fig. 3b and Supplementary Fig. 16). The best fits indicate a gradual increase of the dispersion broadness parameter (α) as temperature is decreased, from 0.3 at 250 K to 0.55 at 180 K (Supplementary Fig. 18). The broadening of the relaxation suggests a larger fraction of interacting dipoles exists when less thermal energy is available. It should be noted, however, that BDS will not detect linkers whose dynamics fall outside the probed frequency range, in particular static linkers, meaning that potential rotation-impeding interactions such as the one illustrated in the DFT curve may not be covered in the dielectric spectra. Fitting the temperature dependence of the mean relaxation times to the Arrhenius equation delivers an activation energy E_a of 32.3 ± 1.3 kJ mol^{-1} and a pre-exponential factor τ_0 of 3.4×10^{-14} s (Supplementary Fig. 19). This activation energy is in between the DFT-estimated barriers for a single unit cell of this framework, i.e., the smaller barrier at 0° and the larger barrier at ca. 90°. The obtained τ_0 value, equivalent to 2.9×10^{13} Hz, is larger than the expected attempt frequency based on estimations for *p*-phenylene rotators (usually on the order of 10^{12} Hz).[25] This type of result is not uncommon for functionalized *p*-phenylene rotors,[30,45,49] and it may be interpreted as an indication of a small linear dependence of the rotational barrier with temperature (see Supplementary Information section 3.5 for further discussion).[50] In NO_2-MIL-53(Al), this could hint towards the progressive effect that thermal energy has on the rotor's environment due to increased conformational motions and nitro group rotations.[51]

To obtain specific information about the angular and frequency ranges of the nitro-functionalized linker dynamics, we performed variable-temperature solid-state deuterium NMR (^{2}H SSNMR) spectroscopy. Spatial information about the deuteron exchange sites can be extracted from the NMR spectra by using relatively simple geometric models.[52,53] In addition, this technique is sensitive to all deuterium-labelled rings, and not only to the mobile ones. This enables us to obtain experimental information to complement the BDS data, especially for the nitro-functionalized framework, for which dynamics above 250 K could not be probed due to the high frequency limit. The results for ring-labelled MIL-53(Al)-d_4 (Supplementary Fig. 20) and NH_2-MIL-53(Al)-d_3 (Supplementary Fig. 21) are in line with literature[42,54,55] as well as our expectations based on the DFT and BDS analyses. The ^{2}H SSNMR data for MIL-53(Al)-d_4 indicate that the phenylene rings undergo an increased rate of 180° reorientations ("π-flips") at increased temperatures in the intermediate motion regime (IMR, 1 kHz < k < 100 MHz, where k is the rate constant for the exchange between deuterium sites). For NH_2-MIL-53(Al)-d_3, only static phenylene ring signals are observed in the slow motion limit (SML, k < 1 kHz), evidenced by the Pake doublet (Supplementary Fig. 21), in line with linker rotation not being possible for this framework.

The variable-temperature ^{2}H SSNMR spectra for NO_2-MIL-53(Al)-d_3 are remarkably different from the aforementioned situations (Fig. 4a). At the lowest temperature, the ^{2}H spectrum indicates a stationary phenylene ring in the SML, whereas the spectra acquired at 409 K and higher indicate dynamics only in the fast motion limit (FML, k > 100 MHz). The spectra in the range of 254 to 387 K display a superposition of the SML and FML powder patterns, with progressive increase in integrated intensity of the FML pattern with respect to the SML pattern with increasing temperature. No pattern corresponding to the IMR was detected in the entire temperature range, differing from earlier ^{2}H SSNMR studies on MOFs with *p*-phenylene rotators;[31,34,35] this is likely due to diminished intensity of IMR spectra when the rates of motion are on the order of the ^{2}H pattern breadths.[56–59] Furthermore, the fact that contributions from both SML and FML patterns are observed across the entire temperature range indicates the presence of a distribution of correlation times for the dynamics, which further obscures signals arising from IMR motions.[36,52,60] Such broad distributions of rotation rates are rarely found in terephthalate MOFs,[8,30,31,34–36] though they are more often observed for *p*-phenylene moieties in polymeric systems,[61–63] where structural heterogeneity among the rotors is often cited as the cause of a wide variety of rotation barriers, and consequently, rotation rates. This observation is further supported by the BDS results: there is a very broad distribution of detected frequencies for each temperature in the BDS spectra for NO_2-MIL-53(Al) (Fig. 3b). As suggested by the DFT calculations, these broad distributions of rotational rates are a consequence of the varied degree of inter-linker steric interactions, which are unique to the nitro-functionalized MOF among the three frameworks.

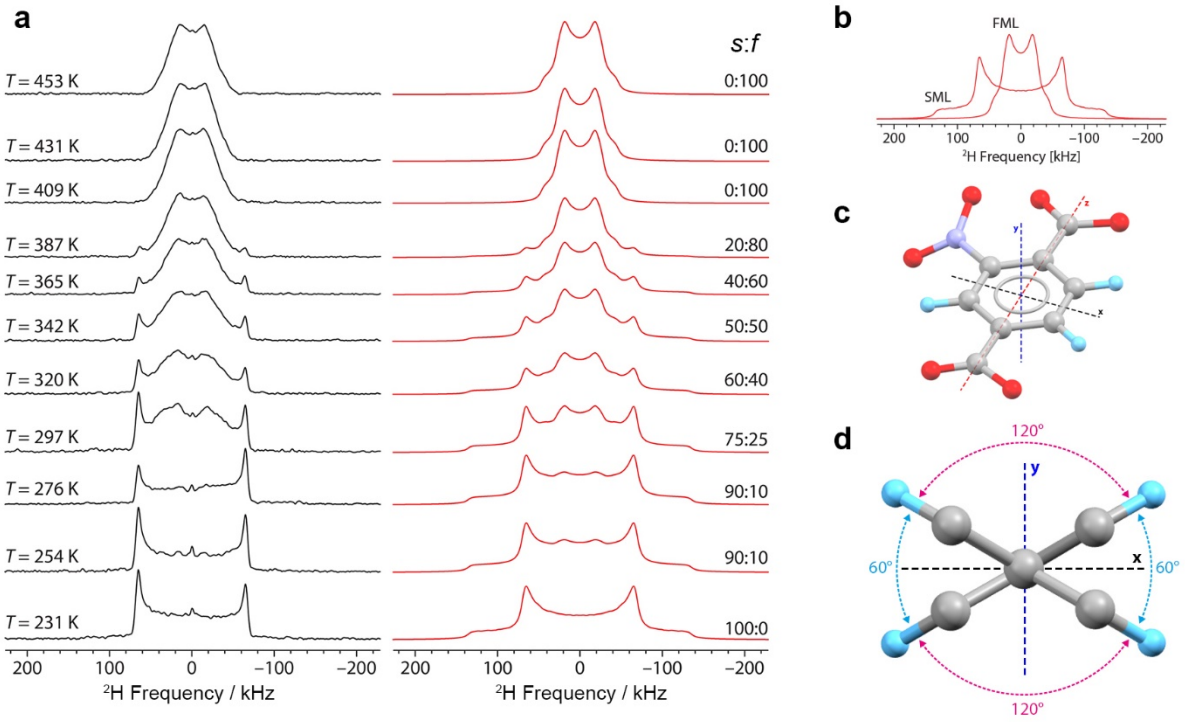

Figure 4. Solid-state ^{2}H NMR studies of NO_2-MIL-53(Al)-d_3. a, Experimental (black) and simulated (red) variable-temperature ^{2}H SSNMR spectra of NO_2-MIL-53(Al)-d_3. **b**, The spectra are comprised of overlapping patterns representing SML (< 10^3 Hz) and FML (> 10^7–10^8 Hz) motions, with relative integrated intensities indicated to the right of the simulated spectra. **c**, Cartesian frame of reference for the rotation model. **d**, Representation of ^{2}H exchange sites and angles used in the model; deuterons are shown in light blue.

Although 2H NMR signals corresponding to motions in the IMR are not observed due to their low intensities and broad frequency distributions, it is possible to model motions in the FML and obtain simulations that agree well with experimental data.[64] Single rotational angle models (e.g., 60°, 120°, or 180°) do not adequately fit the line shape (Supplementary Fig. 22), suggesting a more complex mechanism. A four-site model based on energy minima separated by two distinct jumps of 60° and 120° (as predicted by DFT calculations, Fig. 4c and d) was successful. The simulated ^{2}H FML shape was found to be sensitive to small deviations in these angles (Supplementary Fig. 23). The complete simulated spectra are shown in Fig. 4a. For the overlapped spectra at 254–387 K, the appropriate ratios of weighted integrated signal intensities for static and mobile components were selected (i.e., *s*:*f*, corresponding to the SML and FML patterns, Fig 4b) and are included in Fig. 4a. It should be noted that similar four-site rotations have been observed in *p*-phenylene rotators within branched linkers that cause intra-linker steric interactions.[22,65]

To summarize the NO_2-MIL-53(Al) experimental results, our BDS and ^{2}H SSNMR experiments detect dynamics corresponding to complementary portions of the frequency spectrum. BDS only includes the mobile fraction of linkers up to 1 MHz, which is the mean frequency of motion at ca. 250 K. ^{2}H SSNMR detects all linkers undergoing slow dynamics below 1 kHz as well as all with fast dynamics above ~100 MHz, which go largely unobserved in BDS due to its lower and upper frequency limits. Effectively, the only overlap between the two spectroscopic analyses (i.e., where both methods detect signals) is at 230–250 K. At 250 K, the ^{2}H SSNMR model indicates that a large majority of the linkers are static, which means the BDS peak at 1 MHz omits information on a significant population of linkers. For this reason, the estimated activation energy should be taken as valid only for this fraction of rotors. In the high-temperature region of the ^{2}H SSNMR spectra, we observe no signal from the SML, and that all rotational motion likely exists within the FML. Both sets of data provide clear evidence that the

rotational motions in NO_2-MIL-53(Al) are spread along a very broad frequency range, which is a rare phenomenon that we can attribute to the addition of the bulky nitro substituent.

To understand the observed frequency broadening and the effect of temperature on how neighboring linkers influence rotational motion in NO_2-MIL-53(Al), we performed *ab initio* molecular dynamics (MD) simulations at 300, 450, 700, and 1200 K. The higher temperatures are not directly relevant to the physical situation (NO_2-MIL-53(Al) combusts at ca. 700 K), yet they allow for more rotation events to be observed during shorter simulation times.[66,67] In periodic MD simulations involving a single unit cell (Supplementary Fig. 24), clear preferential conformations are observed, consistent with the potential energy minima observed in zero-Kelvin calculations. At lower temperatures (e.g., 300 K), the linkers undergo discrete 60° rotations between 30° to −30°, whose frequency increases with temperature. At higher temperatures, we also see the occurrence of 120° jumps between ±30° and ±150°. Both motions are consistent with the ^{2}H SSNMR data and the DFT-predicted energy barriers.

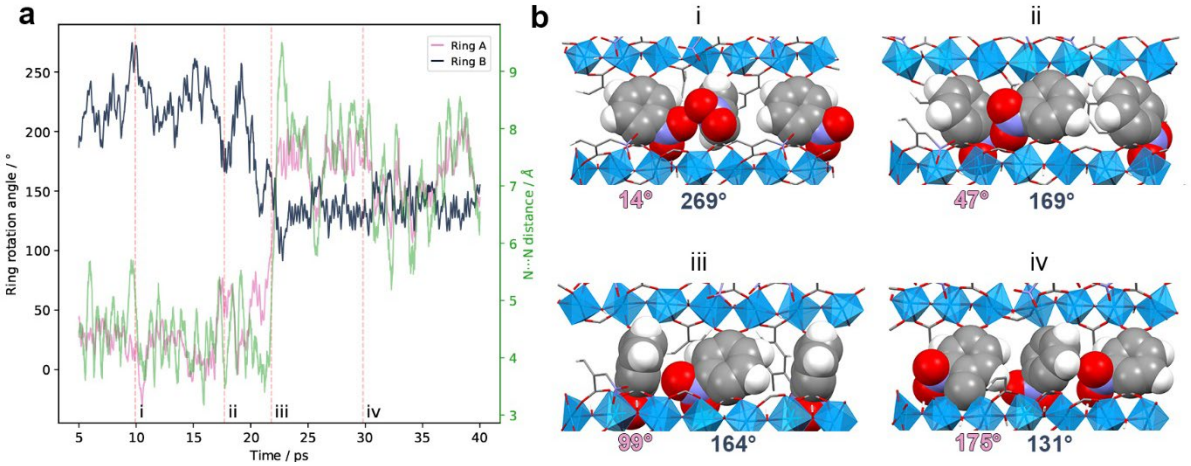

Figure 5. Cooperative rotation in NO_2-MIL-53(Al). a, Rotation angle traces of two neighboring rings in a 2x1x1 cell MD simulation at 700 K. Correlated motion is observed, with simultaneous angle changes in opposite directions (i,ii,iii), when nitro groups are in proximity (N···N distance ca. 4 Å). **b**, Selected snapshots (i-iv) of linker pair conformation during a cooperative rotation. As ring A rotates in the positive direction, ring B reaches the space originally occupied by ring A.

A similar trend in angular mobility ranges is observed for 2x1x1 supercell simulations. At 300 K, only small angle librations ca. 20° are observed (Supplementary Fig. 25). In the mid-temperature range (450-700 K), two sets of rotational jumps appear, in addition to librations (Supplementary Figs. 26–27). At the highest temperature simulated (1200 K), the linkers' motion becomes so fast and extensive that even rotation beyond 180° occurs (Supplementary Fig. 28).

Interestingly, barring the 1200 K simulations, the time traces of rotation angles feature repeated occurrences of apparent correlated fluctuations in both librations and jumps of adjacent linker pairs. This is less evident in the 300 K simulations, where rings did not undergo any large-angle jumps. To analyze the relation between this apparent correlated motion and the steric effect of linkers within a row, we compare the distance between nitro groups of each pair of neighboring linkers (defined as the distance between the two nitrogen atoms, see Supplementary Information section 3.8) with the angle traces at 450 K and 700 K (Figure 5a and Supplementary Figs. 30–33). Indeed, the rings at these temperatures perform mirrored small angle (~ 50°) fluctuations when the distance between their nitro groups is small (Fig. 5b). In the portions of the simulations where the nitro distances are large enough as to not cause steric effects, the mirrored correlated motion is not present, and faster, shorter fluctuations are observed.

Although large-angle jumps are relatively rare in the supercell simulations, Figure 5 and Supplementary Figs. 31 and 33 show examples of correlated large-angle motions that occur when nitro groups are in proximity. A closer analysis of the molecular conformations during a simulation provides a clear example of these cooperative dynamics, presented in Figure 5 and Supplementary Video. The snapshot sequence presented in Figure 5b illustrates how the limited space of the rotors requires cooperative motion to allow the change in angles from i to iv. In this case, ring A could be seen as rotating cooperatively in the positive direction (most noticeable in snapshots ii to iii) allowing ring B to rotate in the negative direction (i–iv), resulting in the pair performing a gearlike rotation. This correlated motion is facilitated by the neighbors' close arrangement, which implies that, in order to achieve certain conformations, cooperative rotation between neighbors is required.

We propose that this type of complex dynamics is in fact what causes NO_2-MIL-53(Al) to display the intriguing behavior determined by BDS and ^{2}H SSNMR analysis. The vast array of possible dynamics observed in this MOF—evidenced by the coexistence of both static and rapidly rotating rings at most temperatures—is a result of functionalizing the phenylene rotators with a substituent that i) drastically decreases the intrinsic rotation barrier and ii) facilitates intra-row steric interactions. Both DFT and ab initio MD methods support the hypothesis that intra-row steric effects lead to cooperative motion for a population of neighboring linkers, while the static rings are the inevitable result of energetically disfavored non-cooperative rotation.

Conclusions

To conclude, the MIL-53 topology, where the distance between the rotational axes of phenylene rings along the pore direction is only ~ 6.6 Å, has proven to be an excellent scaffold in which to tune rotational mobility in different dynamic regimes. At the two extremes, there are (i) unfunctionalized phenylene units that can rotate independently, with specific temperature-dependent rates, and (ii) amino-functionalized phenylene units that cannot rotate at all, due to intralinker hydrogen bonding and increased steric hindrance from the narrow-pore configuration. Between these extremes, for nitrophenylene linkers, we observe complex rotational dynamics that evolve with temperature, spanning a broad frequency range. Among these, we identify for the first time the emergence of cooperative rotational dynamics between neighboring linkers in MOFs. This discovery paves the way to engineering gearlike functional motion in MOFs, if linker dynamics can also be controlled externally, e.g. by electric fields.

Acknowledgements

The work of A.G.-N. forms part of the research program of DPI, NEWPOL project 731.015.506. M.A.v.d.V. and S.M. are grateful for funding by the European Research Council (grant number 759212) within the Horizon 2020 Framework Programme (H2020-EU.1.1). This work was sponsored by NWO Exact and Natural Sciences for the use of supercomputer facilities. R.W.S. is grateful for research support from The Florida State University and the National High Magnetic Field Laboratory (NHMFL), which is funded by the National Science Foundation Cooperative Agreement (DMR-1644779) and by the State of Florida. R.W.S. also acknowledges the support of the Natural Science and Engineering Research Council (NSERC, Canada) through an Research Tools and Instrument (RTI) grant and NSERC Discovery Grant (RGPIN-2016_06642). The authors are grateful to the Canadian Foundation for Innovation (CFI), the Ontario Innovation Trust (OIT) and the University of Windsor for support of solid-state characterization facilities at Windsor. F.-X.C. acknowledges financial support from the Agence

Nationale de la Recherche under project MATAREB (ANR-18-CE29-0009-01) and access to high-performance computing platforms provided by GENCI grant A0070807069.

Author Contributions

M.A.vdV. conceptualized the project. M.A.vdV, A.G.-N., and F.-X.C. designed the study. A.G.-N. performed synthesis, characterization experiments, and DFT calculations. S.M. performed MD simulations. A.G.-N. and S.M. analyzed MD simulation data. M.S. S.B. performed and analyzed BDS under guidance of J.B. C.V. and A.A. collected the SSNMR data. A.A. and R.W.S. analyzed and interpreted SSNMR data. A.G.-N. and M.A.vdV. wrote the manuscript with input from all authors.

Competing Interests

The authors declare no competing interests.

Data Availability

The source data for all figures, raw data from ^{2}H SSNMR experiments, and all DFT/MD-generated structures are available in the 4TU repository, [link and DOI will be provided previous to publication].

Code Availability

The Python code used to analyze the ring rotation angles from MD simulation data is available online at https://github.com/srinidhimula/supplementary-data. A detailed description of the code's functionality is provided in Supplementary Information section 3.9.

References

1. van Meer, G., Voelker, D. R. & Feigenson, G. W. Membrane lipids: where they are and how they behave. *Nat. Rev. Mol. Cell Biol.* **9**, 112–124 (2008).

2. Duncan, A. L. *et al.* Protein crowding and lipid complexity influence the nanoscale dynamic organization of ion channels in cell membranes. *Sci. Rep.* **7**, 16647 (2017).

3. van der Kooij, H. M. *et al.* Morphing of liquid crystal surfaces by emergent collectivity. *Nat. Commun.* **10**, 1–9 (2019).

4. Catalano, L. & Naumov, P. Exploiting rotational motion in molecular crystals. *CrystEngComm* **20**, 5872–5883 (2018).

5. Vogelsberg, C. S. & Garcia-Garibay, M. A. Crystalline molecular machines: function, phase order, dimensionality, and composition. *Chem. Soc. Rev.* **41**, 1892–1910 (2012).

6. Khuong, T.-A. A. V *et al.* Crystalline molecular machines: A quest toward solid-state dynamics and function. *Acc. Chem. Res.* **39**, 413–422 (2006).

7. Deng, H., Olson, M. A., Stoddart, J. F. & Yaghi, O. M. Robust dynamics. *Nat. Chem.* **2**, 439–443 (2010).

8. Gonzalez-Nelson, A., Coudert, F.-X. & van der Veen, M. Rotational Dynamics of Linkers in Metal–Organic Frameworks. *Nanomaterials* **9**, 330 (2019).

9. Martinez-Bulit, P., Stirk, A. J. & Loeb, S. J. Rotors, Motors, and Machines Inside Metal–Organic

Frameworks. *Trends in Chemistry* vol. 1 588–600 (2019).

10. Gee, J. A. & Sholl, D. S. Effect of Framework Flexibility on C 8 Aromatic Adsorption at High Loadings in Metal–Organic Frameworks. *J. Phys. Chem. C* **120**, 370–376 (2016).

11. Park, J. *et al.* Impact of intrinsic framework flexibility for selective adsorption of sarin in non-aqueous solvents using metal–organic frameworks. *Phys. Chem. Chem. Phys.* **22**, 6441–6448 (2020).

12. Agrawal, M. *et al.* Liquid-Phase Multicomponent Adsorption and Separation of Xylene Mixtures by Flexible MIL-53 Adsorbents. *J. Phys. Chem. C* **122**, 386–397 (2018).

13. Verploegh, R. J. *et al.* Screening Diffusion of Small Molecules in Flexible Zeolitic Imidazolate Frameworks Using a DFT-Parameterized Force Field. *J. Phys. Chem. C* **123**, 9153–9167 (2019).

14. Witman, M. *et al.* The Influence of Intrinsic Framework Flexibility on Adsorption in Nanoporous Materials. *J. Am. Chem. Soc.* **139**, 5547–5557 (2017).

15. Lennox, M. J. & Düren, T. Understanding the Kinetic and Thermodynamic Origins of Xylene Separation in UiO-66(Zr) via Molecular Simulation. *J. Phys. Chem. C* **120**, 18651–18658 (2016).

16. Evans, J. D., Krause, S. & Feringa, B. L. Cooperative and synchronized rotation in motorized porous frameworks: Impact on local and global transport properties of confined fluids. *Faraday Discuss.* (2020) doi:10.1039/D0FD00016G.

17. Aprahamian, I. The Future of Molecular Machines. *ACS Cent. Sci.* **6**, 347–358 (2020).

18. Vogelsberg, C. S. *et al.* Ultrafast rotation in an amphidynamic crystalline metal organic framework. *Proc. Natl. Acad. Sci.* **114**, 13613–13618 (2017).

19. Bracco, S. *et al.* Ultrafast Molecular Rotors and Their CO2Tuning in MOFs with Rod-Like Ligands. *Chem. - A Eur. J.* **23**, 11210–11215 (2017).

20. Danowski, W. *et al.* Unidirectional rotary motion in a metal–organic framework. *Nat. Nanotechnol.* **14**, 488–494 (2019).

21. Kottas, G. S., Clarke, L. I., Horinek, D. & Michl, J. Artificial Molecular Rotors. *Chem. Rev.* **105**, 1281–1376 (2005).

22. Yan, Y. *et al.* Porous Metal–Organic Polyhedral Frameworks with Optimal Molecular Dynamics and Pore Geometry for Methane Storage. *J. Am. Chem. Soc.* **139**, 13349–13360 (2017).

23. Sokolov, A. N., Swenson, D. C. & MacGillivray, L. R. Conformational polymorphism in a heteromolecular single crystal leads to concerted movement akin to collective rack-and-pinion gears at the molecular level. *Proc. Natl. Acad. Sci.* **105**, 1794–1797 (2008).

24. Jarowski, P. D., Houk, K. N. & Garcia-Garibay, M. A. Importance of correlated motions on the low barrier rotational potentials of crystalline molecular gyroscopes. *J. Am. Chem. Soc.* **129**, 3110–3117 (2007).

25. Howe, M. E. & Garcia-Garibay, M. A. The Roles of Intrinsic Barriers and Crystal Fluidity in Determining the Dynamics of Crystalline Molecular Rotors and Molecular Machines. *J. Org. Chem.* **84**, 9835–9849 (2019).

26. Lemouchi, C. *et al.* Crystalline Arrays of Pairs of Molecular Rotors: Correlated Motion, Rotational Barriers, and Space-Inversion Symmetry Breaking Due to Conformational

Mutations. *J. Am. Chem. Soc.* **135**, 9366–9376 (2013).

27. Damron, J. T. *et al.* The Influence of Chemical Modification on Linker Rotational Dynamics in Metal–Organic Frameworks. *Angew. Chemie - Int. Ed.* **57**, 8678–8681 (2018).

28. Zhou, W. & Yildirim, T. Lattice dynamics of metal-organic frameworks: Neutron inelastic scattering and first-principles calculations. *Phys. Rev. B* **74**, 180301 (2006).

29. Ryder, M. R. *et al.* Detecting Molecular Rotational Dynamics Complementing the Low-Frequency Terahertz Vibrations in a Zirconium-Based Metal-Organic Framework. *Phys. Rev. Lett.* **118**, 1–6 (2017).

30. Liepuoniute, I. *et al.* Enhanced Rotation by Ground State Destabilization in Amphidynamic Crystals of a Dipolar 2,3-Difluorophenylene Rotator as Established by Solid State 2 H NMR and Dielectric Spectroscopy. *J. Phys. Chem. C* **124**, 15391–15398 (2020).

31. Kolokolov, D. I. *et al.* Dynamics of benzene rings in MIL-53(Cr) and MIL-47(V) frameworks studied by2H NMR spectroscopy. *Angew. Chemie - Int. Ed.* **49**, 4791–4794 (2010).

32. Kolokolov, D. I., Stepanov, A. G. & Jobic, H. Guest controlled rotational dynamics of terephthalate phenylenes in metal-organic framework MIL-53(Al): Effect of different xylene loadings. *J. Phys. Chem. C* **118**, 15978–15984 (2014).

33. Khudozhitkov, A. E. *et al.* Ultraslow Dynamics of a Framework Linker in MIL-53 (Al) as a Sensor for Different Isomers of Xylene. *J. Phys. Chem. C* **120**, 21704–21709 (2016).

34. Khudozhitkov, A. E., Kolokolov, D. I., Stepanov, A. G., Bolotov, V. A. & Dybtsev, D. N. Metal-Cation-Independent Dynamics of Phenylene Ring in Microporous MOFs: A 2H Solid-State NMR Study. *J. Phys. Chem. C* **119**, 28038–28045 (2015).

35. Gould, S. L., Tranchemontagne, D., Yaghi, O. M. & Garcia-Garibay, M. A. Amphidynamic character of crystalline MOF-5: Rotational dynamics of terephthalate phenylenes in a free-volume, sterically unhindered environment. *J. Am. Chem. Soc.* **130**, 3246–3247 (2008).

36. Kolokolov, D. I. *et al.* Probing the dynamics of the porous Zr terephthalate UiO-66 framework using 2H NMR and neutron scattering. *J. Phys. Chem. C* **116**, 12131–12136 (2012).

37. Biswas, S., Ahnfeldt, T. & Stock, N. New functionalized flexible Al-MIL-53-X (X = -Cl, -Br, -CH 3, -NO 2, -(OH) 2) solids: Syntheses, characterization, sorption, and breathing behavior. *Inorg. Chem.* **50**, 9518–9526 (2011).

38. Loiseau, T. *et al.* A rationale for the large breathing of the porous aluminum terephthalate (MIL-53) upon hydration. *Chemistry* **10**, 1373–1382 (2004).

39. Munn, A. S. *et al.* The flexibility of modified-linker MIL-53 materials. *Dalt. Trans.* **45**, 4162–4168 (2016).

40. Stavitski, E. *et al.* Complexity behind CO2 capture on NH2-MIL-53(Al). *Langmuir* **27**, 3970–3976 (2011).

41. Shustova, N. B. *et al.* Phenyl Ring Dynamics in a Tetraphenylethylene-Bridged Metal–Organic Framework: Implications for the Mechanism of Aggregation-Induced Emission. *J. Am. Chem. Soc.* **134**, 15061–15070 (2012).

42. Kolokolov, D. I., Stepanov, A. G. & Jobic, H. SI: Guest controlled rotational dynamics of terephthalate phenylenes in metal-organic framework MIL-53(Al): Effect of different xylene

loadings. *J. Phys. Chem. C* **118**, 15978–15984 (2014).

43. Balčiūnas, S. *et al.* Low-Frequency Dipolar Dynamics and Atmospheric Effects in ZIF-90 Metal–Organic Framework. *J. Phys. Chem. C* **123**, 631–636 (2019).

44. Winston, E. B. *et al.* Dipolar molecular rotors in the metal–organic framework crystal IRMOF-2. *Phys. Chem. Chem. Phys.* **10**, 5188 (2008).

45. Devautour-Vinot, S. *et al.* Structure and dynamics of the functionalized MOF type UiO-66(Zr): NMR and dielectric relaxation spectroscopies coupled with DFT calculations. *Chem. Mater.* **24**, 2168–2177 (2012).

46. Kremer, F. & Schonhals, A. *Broadband Dielectric Spectroscopy*. (Springer-Verlag: Berlin, Heidelberg, 2003).

47. Frunza, S. *et al.* Molecular relaxation processes in a MOF-5 structure revealed by broadband dielectric spectroscopy: Signature of phenylene ring fluctuations. *J. Phys. Chem. B* **114**, 12840–12846 (2010).

48. Knebel, A. *et al.* Defibrillation of soft porous metal-organic frameworks with electric fields. *Science* **358**, 347–351 (2017).

49. Horansky, R. D. *et al.* Dielectric response of a dipolar molecular rotor crystal. *Phys. Rev. B - Condens. Matter Mater. Phys.* **72**, 1–5 (2005).

50. Horansky, R. D. *et al.* Dipolar rotor-rotor interactions in a difluorobenzene molecular rotor crystal. *Phys. Rev. B - Condens. Matter Mater. Phys.* **74**, 1–12 (2006).

51. Jiang, X. *et al.* Crystal Fluidity Reflected by Fast Rotational Motion at the Core, Branches, and Peripheral Aromatic Groups of a Dendrimeric Molecular Rotor. *J. Am. Chem. Soc.* **138**, 4650–4656 (2016).

52. Hansen, M. R., Graf, R. & Spiess, H. W. Solid-State NMR in Macromolecular Systems: Insights on How Molecular Entities Move. *Acc. Chem. Res.* **46**, 1996–2007 (2013).

53. Spiess, H. W. Molecular dynamics of solid polymers as revealed by deuteron NMR. *Colloid Polym. Sci* **261**, 193–209 (1983).

54. Khudozhitkov, A. E. *et al.* Ultraslow Dynamics of a Framework Linker in MIL-53 (Al) as a Sensor for Di ff erent Isomers of Xylene. **53**, (2016).

55. Serra-Crespo, P. *et al.* NH2-MIL-53(Al): A high-contrast reversible solid-state nonlinear optical switch. *J. Am. Chem. Soc.* **134**, 8314–8317 (2012).

56. Spiess, H. W. Deuteron NMR — a new tool for studying chain mobility and orientation in polymers. in 23–58 (1985). doi:10.1007/3-540-13779-3_16.

57. Gedat, E. *et al.* 2H-solid-state NMR study of benzene-d6confined in mesoporous silica SBA-15. *J. Phys. Chem. B* **106**, 1977–1984 (2002).

58. Larsen, F. H. Simulation of Molecular Motion of Quadrupolar Nuclei in Solid-State NMR Spectra. in *Annual Reports on NMR Spectroscopy* vol. 71 103–137 (Elsevier Ltd, 2010).

59. Aliev, A. E. *et al.* High-Resolution Solid-State H-2 NMR Spectroscopy of Polymorphs of Glycine. *J. Phys. Chem. A* **115**, 12201–12211 (2011).

60. Schadt, R. J., Cain, E. J. & English, A. D. Simulation of one-dimensional deuteron NMR line shapes. *J. Phys. Chem.* **97**, 8387–8392 (1993).

61. Leisen, J., Ohlemacher, A., Boeffel, C. & Spiess, H. W. Molecular Dynamics in Side-Group Polymers with and without Liquid Crystalline Phases from 2H NMR. *Berichte der Bunsengesellschaft für Phys. Chemie* **97**, 1306–1311 (1993).

62. Pschorn, U., Spiess, H. W., Hisgen, B. & Ringsdorf, H. Deuteron NMR study of molecular order and motion of the mesogenic side groups in liquid-crystalline polymers. *Die Makromol. Chemie* **187**, 2711–2723 (1986).

63. Wehrle, M., Hellmann, G. P. & Spiess, H. W. Phenylene motion in polycarbonate and polycarbonate/additive mixtures. *Colloid Polym. Sci.* **265**, 815–822 (1987).

64. Wasylishen, R. E., Ashbrook, S. E. & Wimperis, S. *NMR of Quadrupolar Nuclei in Solid Materials*. (John Wiley & Sons, 2012).

65. Moreau, F. *et al.* Tailoring porosity and rotational dynamics in a series of octacarboxylate metal-organic frameworks. *Proc. Natl. Acad. Sci.* **114**, 3056–3061 (2017).

66. Haigis, V., Coudert, F.-X., Vuilleumier, R., Boutin, A. & Fuchs, A. H. Hydrothermal Breakdown of Flexible Metal–Organic Frameworks: A Study by First-Principles Molecular Dynamics. *J. Phys. Chem. Lett.* **6**, 4365–4370 (2015).

67. Gaillac, R. *et al.* Liquid metal–organic frameworks. *Nat. Mater.* **16**, 1149–1155 (2017).